



Nonlinear forced vibrations of three-phase nanocomposite shells considering matrix rheological behavior and nano-fiber waviness

R. Nopour¹ · F. Ebrahimi² · A. Dabbagh³ · M. M. Aghdam¹

Received: 4 November 2021 / Accepted: 14 January 2022 / Published online: 7 February 2022
© The Author(s), under exclusive licence to Springer-Verlag London Ltd., part of Springer Nature 2022

Abstract

The present study investigates the nonlinear vibrations in thin-walled shells consisting of three-phase polymer nanocomposites with regard to the viscoelastic properties of polymer and curved shape of carbon nanotubes (CNTs). To this end, a hierarchical micromechanical framework is introduced to study the effective properties of multi-scale hybrid (MSH) nanocomposite. Next, the von Kármán-type nonlinearity is considered together with the displacement field of the classical shell theory to derive the governing equations in the context of Hamilton's principle. In addition, the impacts of both axial compression and transverse harmonic stimulation on the dynamic response of the system are taken into consideration. Afterward, the method of harmonic balance is implemented to find the frequency–response relation of the structure. The transient response is also achieved with the aid of fourth-order Runge–Kutta method. The results of this work reveal that resonance estimation in such hybrid nanomaterial structures will be inaccurate if the softening effect of waviness phenomenon on the modulus is ignored. On one hand, it is demonstrated that the amplitude of the dynamic deflection of the shell will be reduced with time (i.e., due to the viscoelastic properties of the polymer). On the other hand, it is depicted that rising the content of glass fibers (GFs) in the MSH nanocomposite shell results in softer oscillations. The reason for this trend is the reducing impact of this change on the content of the CNTs in the composition of the polymer nanocomposite.

Keywords Multi-scale hybrid nanocomposite · Viscoelastic material · Waviness phenomenon · Nonlinear vibrations · Thin-walled shells

1 Introduction

Since the invention of carbon nanotubes (CNTs) in the 1990s [1], various nano-engineered devices were designed thanks to the outstanding properties of nanosize elements [2, 3]. In other words, the enhanced ultimate stiffness and strength, high slenderness ratio, light weight, and high thermal conductivity of CNTs [4] have made them key elements in the

design of critical instruments. Therefore, implementation of CNTs for the purpose of reinforcing polymers can be an efficient means to design structural elements. Keeping this fact in mind, many studies can be addressed whose major concern is to monitor the reaction of CNT-reinforced (CNTR) nanocomposite structures, in different working conditions, to mechanical stimulations [5–42]. Even though these studies provided rough data about the general behaviors of CNTR polymers, their findings seem to be engineering overestimations because of the fact that practical aspects of designing nanocomposites exist in none of them. In other words, all of the above studies were accomplished by assuming the CNTR polymer to be like a fiber-reinforced one. However, this ideal assumption cannot be satisfied in such polymer nanocomposites. This mismatch has several reasons, among them the wavy shape of CNTs (i.e., reported to originate from high slenderness ratio of the CNTs, their topological defect, and existing van der Waals (vdW) forces between them [43, 44]) is of high significance. To capture this issue while tracking the stress–strain curve of the CNTR polymers, a

✉ F. Ebrahimi
febrahimi@eng.ikiu.ac.ir

¹ Department of Mechanical Engineering, Amirkabir University of Technology, Hafez Ave., 15875-4413 Tehran, Iran

² Department of Mechanical Engineering, Faculty of Engineering, Imam Khomeini International University, Noroozian Blvd, 34148-96818 Qazvin, Iran

³ School of Mechanical Engineering, College of Engineering, University of Tehran, North Kargar St, 11155-4563 Tehran, Iran

semi-empirical attempt was made in [45]. According to this study, a modified homogenization technique for accurate estimation of the Young's modulus of CNTR polymers was attained. In addition to the waviness phenomenon, formation of CNT agglomerates in the microstructure of a CNTR polymer weakens the reinforcing power of such nanofillers. To cover this issue, a gradual distribution of the agglomerated CNTs across the thickness direction was introduced in another micromechanics-assisted study [46]. In this work, the entanglement of the CNTs inside the inclusions was kept in mind while the Young's modulus of the CNTR nanocomposite was calculated. Recently, the effect of temporal degradation of the properties of polymer on the approximation of modulus in nanocomposites has been covered in another micromechanical investigation [47].

In the above-mentioned studies, bi-phase nanocomposites consisting of polymer and CNT were discussed. Recent studies, however, have shown that three-phase nanocomposites, referred to as multi-scale hybrid (MSH) nanocomposites, have potential to better match the design criteria in the field of structural mechanics. In these hybrid nanomaterials, the third phase belongs to macro-scale fibers such as glass or carbon fibers (GFs/CFs). In the middle 2010s, some researchers started to analyze static and dynamic behaviors of MSH nanocomposite structures. In one of the initial efforts in this area, first-order shear deformation theory (FSDT) was hired to probe nonlinear free vibration behaviors of rectangular sandwich plates made of smart piezoelectric MSH nanomaterials [48]. By means of a rheological solid element, the viscoelastically damped oscillations of sandwich beams consisting of MSH nanocomposites were tracked in [49]. Investigation of the nonlinear dynamic properties of MSH nanocomposite blades was done in [50] once the nanomaterial-made blade seemed to be rotating around its longitudinal axis. In another geometrically nonlinear study, finite element method (FEM) was employed in [51] to probe low-velocity impact features of MSH nanocomposite plates positioned in a hygrothermal environment. According to the classical theory of thin beams, nonlinear deflection, critical postbuckling temperature, and bifurcation properties of MSH nanocomposite beams were determined in [52] via simple Halpin–Tsai homogenization algorithm. Using the well-known Rayleigh–Ritz FE solution, the modal characteristics of MSH nanocomposite thick beams were studied in [53]. In another endeavor, the same authors surveyed the bi-axial buckling problem of rectangular plates consisting of MSH nanocomposites [54] in the framework of classical theory of thin plates. Lately, the destroying influence of the CNT agglomerates on the buckling-mode failure and oscillation frequency of MSH nanocomposite structures was covered in [55–57] and [58, 59], respectively.

Based on the above literature review, it can be easily realized that the impacts of wavy shape of the CNTs and

time-varying modulus of the polymer on the dynamic characteristics of MSH nanocomposite structures have not been paid enough attention. In the solitary work in this field, the vibrational behaviors of viscoelastic three-phase nanocomposite plates were studied in [60]. To cover this lack in the literature and by recalling the broad application of nanocomposite shells as aerospace structures, structural devices, marine structures, energy storage devices, highly sensitive strain sensors, etc., we decided to probe the nonlinear vibration of MSH nanocomposite thin-walled shells subjected to a hard-type harmonic stimulation. In this regard, the viscoelastic properties of the matrix will be considered to be like that expressed in [47]. Afterward, the modified version of the Halpin–Tsai method will be implemented to consider the effect of curved shape of the nanofillers on the dynamic response of the continuous system. Next, the classical theory of thin cylindrical shells will be mixed with the nonlinear strain–displacement relations of von Kármán to derive the nonlinear governing equations of the system with the aid of an energy method. Finally, the problem will be solved analytically and both tabular and illustrative case studies will be depicted for reference.

2 Theory and formulation

2.1 Micromechanical homogenization

Here, the equivalent properties of MSH nanocomposite will be obtained. The schematic flowchart implemented for modeling the hybrid nanocomposite can be found in Fig. 1. The MSH nanocomposite is assumed to be hosted by a polymer whose time-varying properties are reported in the literature. Polymers promote viscoelastic behavior in various working conditions [61]. Thus, it is logical to consider the properties of such soft materials to be time varying [62]. In this study, an exponential temporal degradation for the polymer's properties will be considered, in accordance with the well-known viscoelastic model of Maxwell [47, 63]. Based on this method, the modulus and Poisson's ratio of the polymer can be calculated via [60]:

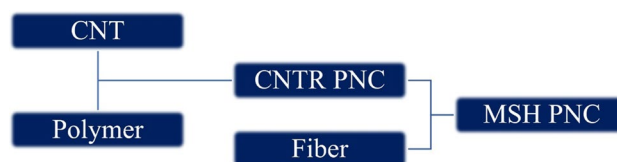


Fig. 1 Schematic flowchart of modeling of the MSH polymer nanocomposites

$$E_{PM}(t) = E_{PM}^0 \exp\left(-\frac{t}{\tau_v}\right)^{\beta_v}, \tag{1}$$

$$v_{PM}(t) = 0.5 - (0.5 - v_{PM}^0) \exp\left(-\frac{t}{\tau_v}\right)^{\beta_v}, \tag{2}$$

where E_{PM}^0 and v_{PM}^0 are the instantaneous elastic modulus at the initial time and initial value of Poisson’s ratio, respectively. The parameters β_v and τ_v are stretching exponent and characteristic relaxation time, respectively. It is worth mentioning that the mass density of the polymer does not vary with time and, thus, it can be stated that $\rho_{PM} = \rho_{PM}^0$.

Next, the equivalent properties of CNTR polymer must be gathered. To this end and with regard to the important influence of the waviness phenomenon on the modulus determination in nanocomposites, the semi-empirical modified Halpin–Tsai method [45] is chosen. Prior to discussing about the homogenization method, it must be declared that the present modeling is based on the fact that a limited content of CNTs is utilized in the composition of the hybrid nanomaterial. If CNT loadings above 2 wt.% are purposed, the present model is not reliable. This issue does not seem important herein, because it is not logical to use CNT loadings of as high as 2 wt.% or more due to the high probability of aggregation phenomenon in such CNT loadings. Once CNTR polymers with low reinforcement content are studied, the present model can be trusted due to the excellent agreement between model predictions and those of experiments [45]. Following this algorithm, the Young’s modulus of the CNTR nanocomposite can be computed as:

$$E_{NCM} = \frac{1 + C\eta V_{CNT}}{1 - \eta V_{CNT}} E_{PM}, \tag{3}$$

where

$$\eta = \frac{C_w [\alpha E_{CNT}/E_{PM}] - 1}{C_w [\alpha E_{CNT}/E_{PM}] + C}, \tag{4}$$

$$C = 2 \frac{l_{CNT}}{d_{CNT}}, \tag{5}$$

in which α is the orientation factor that must be set to 1/6 due to very small dimensions of the CNTs in comparison with the entire thickness of the structure [64]. In addition, C is a geometry-based coefficient which is in charge of capturing the shape of nanofillers. Finally, the sign C_w stands for the waviness coefficient which is defined as $C_w = 1 - a/w$. In this definition, a and w are amplitude and range of the wave existing in the CNT, respectively. It is worth mentioning that the introduced waviness coefficient varies between zero and one where the CNTs are assumed to be like circle

(fully curved CNTs) and string (ideal CNTs), respectively. Also, the mass density and Poisson’s ratio of the CNTR nanocomposite can be achieved using [60]:

$$\rho_{NCM} = \rho_{CNT} V_{CNT} + \rho_{PM} V_{PM}, \tag{6}$$

$$v_{NCM} = v_{CNT} V_{CNT} + v_{PM} V_{PM}. \tag{7}$$

Once Eqs. (3) and (7) are mixed, the shear modulus of the CNTR polymer will be obtained via $G_{NCM} = E_{NCM}/2(1 + v_{NCM})$. In Eqs. (3), (6), and (7), the volume fraction of the CNTs can be gathered by [60]:

$$V_{CNT} = \left(\frac{\rho_{CNT}}{m_r \rho_{PM}} - \frac{\rho_{CNT}}{\rho_{PM}} + 1\right)^{-1}, \tag{8}$$

where ρ_{CNT} and ρ_{PM} , respectively, correspond to the mass densities of CNTs and polymer. Also, m_r is the mass fraction of the nanofillers.

At this stage, we find the equivalent properties of the MSH nanomaterial. To do so, assume a fiber-reinforced composite whose matrix is the CNTR polymer. In this paper, GFs are employed as the reinforcing macro-scale fiber. If the Young’s modulus, shear modulus, and Poisson’s ratio of the GFs are, respectively, E_F , G_F , and v_F , the effective properties of MSH nanocomposite can be achieved using [60]:

$$E_{11} = E_F V_F + E_{NCM} V_{PM}^*, \tag{9}$$

$$E_{22} = E_{33} = \frac{E_{NCM}}{1 - V_F(1 - E_{NCM}/E_F)}, \tag{10}$$

$$G_{12} = G_{13} = G_{23} = \frac{G_{NCM}}{1 - V_F(1 - G_{NCM}/G_F)}, \tag{11}$$

$$v_{12} = v_{13} = v_F V_F + v_{NCM} V_{PM}^*, \tag{12}$$

$$v_{23} = \frac{E_{22}}{2G_{23}} - 1, \tag{13}$$

in which E_{11} , E_{22} , and E_{33} stand for Young’s modulus in the axial, transverse, and flexural directions, respectively. Besides, in- and out-of-plane shear modules are shown with G_{12} , G_{13} , and G_{23} . The signs v_{12} , v_{13} , and v_{23} indicate the Poisson’s ratios in different planes. It is worth mentioning that in Eqs. (9)–(12), the GFs’ volume fraction V_F (i.e., identical to $1 - V_{PM}^*$) can be defined as [60]:

$$V_F = \left(\frac{\rho_F}{m_f \rho_{NCM}} - \frac{\rho_F}{\rho_{NCM}} + 1\right)^{-1}. \tag{14}$$

In the above definition, m_f denotes GFs’ mass fraction.

2.2 Classical shell theory

The present section of this article is dedicated to derivation of the kinematic relations describing the problem. There exist different kinematic theories for mathematical description of structures' motion in the solid mechanics. Generally, these theories can be categorized into three classical [65–68], first-order [69–71], and higher-order [72–74] theories whose main objective is to simulate thin, moderately thick, and thick structures, respectively. Due to the fact that shear deformation can be ignored in the investigation of thin structures [75, 76], classical theory of thin-walled cylindrical shells is selected in this study. By considering the axial displacement, circumferential one, and bending deformation shown by u , v , and w , respectively, and keeping the von Kármán-type geometrical nonlinearity in mind, the nonvanishing components of the strain tensor can be presented as [77]:

$$\begin{aligned} \epsilon_{xx} &= \epsilon_x^0 - z\kappa_x, \\ \epsilon_{yy} &= \epsilon_y^0 - z\kappa_y, \\ \gamma_{xy} &= \gamma_{xy}^0 - 2z\kappa_{xy}. \end{aligned} \tag{15}$$

In the above definitions, normal (ϵ_x^0 and ϵ_y^0) and in-plane shear (γ_{xy}^0) strains are [77]:

$$\begin{aligned} \epsilon_x^0 &= \frac{\partial u}{\partial x} + \frac{1}{2} \left(\frac{\partial w}{\partial x} \right)^2, \\ \epsilon_y^0 &= \frac{\partial v}{\partial y} - \frac{w}{R} + \frac{1}{2} \left(\frac{\partial w}{\partial y} \right)^2, \\ \gamma_{xy}^0 &= \frac{\partial v}{\partial x} + \frac{\partial u}{\partial y} + \frac{\partial w}{\partial x} \frac{\partial w}{\partial y}. \end{aligned} \tag{16}$$

Also, longitudinal (κ_x) and circumferential (κ_y) curvatures and the in-plane twist (κ_{xy}) are [77]:

$$\begin{aligned} \kappa_x &= \frac{\partial^2 w}{\partial x^2}, \\ \kappa_y &= \frac{1}{R} \frac{\partial v}{\partial y} + \frac{\partial^2 w}{\partial y^2}, \\ \kappa_{xy} &= \frac{1}{2R} \frac{\partial v}{\partial x} + \frac{\partial^2 w}{\partial x \partial y}, \end{aligned} \tag{17}$$

where $y = R\theta$.

2.3 Constitutive equations

Herein, the Hook's law for linearly elastic solids will be hired to find a suitable relationship between forces, moments, and displacement field components. According to this rule, the Cauchy stress and strain tensors can be

related to each other via $\sigma_{ij} = C_{ijkl}\epsilon_{kl}$. In this identity, the corresponding arrays of Cauchy stress and strain tensors are shown with σ_{ij} and ϵ_{kl} , respectively, whereas C_{ijkl} indicates the corresponding array of the elasticity tensor. If the plane stress condition is considered, the above-mentioned identity can be re-written as follows [78]:

$$\begin{Bmatrix} \sigma_{xx} \\ \sigma_{yy} \\ \sigma_{xy} \end{Bmatrix} = \begin{bmatrix} Q_{11} & Q_{12} & 0 \\ Q_{12} & Q_{22} & 0 \\ 0 & 0 & Q_{66} \end{bmatrix} \begin{Bmatrix} \epsilon_{xx} \\ \epsilon_{yy} \\ \gamma_{xy} \end{Bmatrix}, \tag{18}$$

where

$$\begin{aligned} Q_{11} &= \frac{E_{11}}{1 - \nu_{12}\nu_{21}}, & Q_{12} &= \frac{\nu_{12}E_{22}}{1 - \nu_{12}\nu_{21}}, \\ Q_{22} &= \frac{E_{22}}{1 - \nu_{12}\nu_{21}}, & Q_{66} &= \frac{E_{11}}{2(1 + \nu_{12})}. \end{aligned} \tag{19}$$

Now, if the forces and moments are assumed to be defined in the following through-the-thickness form (N_{ij}, M_{ij}) = $\int_{-h/2}^{h/2} (1, z)\sigma_{ij}dz$, ($i, j = x, y$) and Eq. (18) is integrated over the thickness of the structure, the following expression can be attained:

$$\begin{Bmatrix} N_x \\ N_y \\ N_{xy} \\ M_x \\ M_y \\ M_{xy} \end{Bmatrix} = \begin{bmatrix} A_{11} & A_{12} & 0 & B_{11} & B_{12} & 0 \\ A_{12} & A_{22} & 0 & B_{12} & B_{22} & 0 \\ 0 & 0 & A_{66} & 0 & 0 & B_{66} \\ B_{11} & B_{12} & 0 & D_{11} & D_{12} & 0 \\ B_{12} & B_{22} & 0 & D_{12} & D_{22} & 0 \\ 0 & 0 & B_{66} & 0 & 0 & D_{66} \end{bmatrix} \begin{Bmatrix} \epsilon_x^0 \\ \epsilon_y^0 \\ \gamma_{xy}^0 \\ -\kappa_x \\ -\kappa_y \\ -2\kappa_{xy} \end{Bmatrix}. \tag{20}$$

In the above identity, through-the-thickness rigidities of the shell can be expressed as:

$$[A_n, B_n, D_n] = \int_{-h/2}^{h/2} [1, z, z^2]Q_n(z)dz, \quad n = (11, 12, 22, 66). \tag{21}$$

2.4 Governing equations

Within this section, the energy method will be implemented for the goal of deriving the motion equations of thin-walled cylindrical shell. To this goal, the dynamic form of the principle of virtual work will be utilized. According to this principle, the variation of the continuous system's Lagrangian, i.e., defined as $L = U + V - T$ (U and T stand for strain and kinetic energies, respectively, and V denotes the work done on the system by external

loadings), over any desired time interval must be set to zero [78, 79]. Following this principle as well as considering the kinematic relations of classical shells, the Euler–Lagrange equations can be derived [77]:

$$\frac{\partial N_x}{\partial x} + \frac{\partial N_{xy}}{\partial y} = I_0 \frac{\partial^2 u}{\partial t^2}, \tag{22}$$

$$\frac{\partial N_{xy}}{\partial x} + \frac{\partial N_y}{\partial y} - \frac{1}{R} \left(\frac{\partial M_{xy}}{\partial x} + \frac{\partial M_y}{\partial y} \right) = I_0 \frac{\partial^2 v}{\partial t^2}, \tag{23}$$

$$\begin{aligned} &\frac{\partial^2 M_x}{\partial x^2} + 2 \frac{\partial^2 M_{xy}}{\partial x \partial y} + \frac{\partial^2 M_y}{\partial y^2} - \frac{N_x}{R} + \frac{\partial}{\partial x} \left(N_x \frac{\partial w}{\partial x} + N_{xy} \frac{\partial w}{\partial y} \right) \\ &+ \frac{\partial}{\partial x} \left(N_{xy} \frac{\partial w}{\partial x} + N_y \frac{\partial w}{\partial y} \right) - ph \frac{\partial^2 w}{\partial x^2} + q = I_0 \frac{\partial^2 w}{\partial t^2} + 2\epsilon I_0 \frac{\partial w}{\partial t}. \end{aligned} \tag{24}$$

In the above set of equations, the in-plane through-the-thickness inertia of the shell can be calculated via:

$$I_0 = \int_{-h/2}^{h/2} \rho dz. \tag{25}$$

In Eqs. (22)–(24), p and q are the axial compression and external distributed load, respectively. In addition, ϵ stands for the damping coefficient of the viscose damper below the structure. Now, the above motion equations must be presented in terms of the components of the displacement field to achieve the governing equations. To this purpose, substitution of Eq. (20) into Eqs. (22)–(24) yields:

$$L_{11}(u) + L_{12}(v) + L_{13}(w) + P_1(w) = I_0 \frac{\partial^2 u}{\partial t^2}, \tag{26}$$

$$L_{21}(u) + L_{22}(v) + L_{23}(w) + P_2(w) = I_0 \frac{\partial^2 v}{\partial t^2}, \tag{27}$$

$$\begin{aligned} &L_{31}(u) + L_{32}(v) + L_{33}(w) + P_3(w) + Q_3(u, w) + R_3(v, w) \\ &- ph \frac{\partial^2 w}{\partial x^2} + q = I_0 \frac{\partial^2 w}{\partial t^2} + 2\epsilon \frac{\partial w}{\partial t}, \end{aligned} \tag{28}$$

where $L_{ij}(\cdot)$ linear operators can be expressed in the following form:

$$\begin{aligned} L_{11}(u) &= A_{11} \frac{\partial^2 u}{\partial x^2} + A_{66} \frac{\partial^2 u}{\partial y^2}, \\ L_{12}(v) &= \left(A_{12} + A_{66} - \frac{B_{12} + B_{66}}{R} \right) \frac{\partial^2 v}{\partial x \partial y}, \\ L_{13}(w) &= -\frac{A_{12}}{R} \frac{\partial w}{\partial x} - B_{11} \frac{\partial^3 w}{\partial x^3} - (B_{12} + 2B_{66}) \frac{\partial^3 w}{\partial x \partial y^2}, \\ L_{21}(u) &= \left(A_{12} + A_{66} - \frac{B_{12} + B_{66}}{R} \right) \frac{\partial^2 u}{\partial x \partial y}, \\ L_{22}(v) &= \left(A_{66} - \frac{2B_{66}}{R} + \frac{D_{66}}{R^2} \right) \frac{\partial^2 v}{\partial x^2} + \left(A_{11} - \frac{2B_{11}}{R} + \frac{D_{11}}{R^2} \right) \frac{\partial^2 v}{\partial y^2}, \\ L_{23}(w) &= -\left(\frac{A_{11}}{R} - \frac{B_{11}}{R^2} \right) \frac{\partial w}{\partial y} - \left(B_{11} - \frac{D_{11}}{R} \right) \frac{\partial^3 w}{\partial y^3} - \left(B_{12} + 2B_{66} - \frac{D_{12} + 2D_{66}}{R} \right) \frac{\partial^3 w}{\partial x^2 \partial y}, \\ L_{31}(u) &= \frac{A_{21}}{R} \frac{\partial u}{\partial x} + B_{11} \frac{\partial^3 u}{\partial x^3} + (B_{12} + 2B_{66}) \frac{\partial^3 u}{\partial x \partial y^2}, \\ L_{32}(v) &= \left(\frac{A_{11}}{R} - \frac{B_{11}}{R^2} \right) \frac{\partial v}{\partial y} + \left(B_{11} - \frac{D_{11}}{R} \right) \frac{\partial^3 v}{\partial y^3} + \left(B_{12} + 2B_{66} - \frac{D_{12} + 2D_{66}}{R} \right) \frac{\partial^3 v}{\partial x^2 \partial y}, \\ L_{33}(w) &= -\frac{A_{11}}{R^2} w - \frac{2A_{12}}{R} \frac{\partial^2 w}{\partial x^2} - \frac{2B_{12}}{R} \frac{\partial^2 w}{\partial y^2} - D_{11} \left(\frac{\partial^4 w}{\partial x^4} + \frac{\partial^4 w}{\partial y^4} \right) - 2(D_{12} + 2D_{66}) \frac{\partial^4 w}{\partial x^2 \partial y^2}. \end{aligned} \tag{29}$$

In addition, the nonlinear operators $P_i(\cdot)$, $Q_3(\cdot)$, and $R_3(\cdot)$ can be defined as:

$$P_1(w) = A_{11} \frac{\partial w}{\partial x} \frac{\partial^2 w}{\partial x^2} + (A_{12} + A_{66}) \frac{\partial w}{\partial y} \frac{\partial^2 w}{\partial x \partial y} + A_{66} \frac{\partial w}{\partial x} \frac{\partial^2 w}{\partial y^2}, \quad (30)$$

$$P_2(w) = \left(A_{66} - \frac{B_{66}}{R} \right) \frac{\partial w}{\partial y} \frac{\partial^2 w}{\partial x^2} + \left(A_{11} - \frac{B_{11}}{R} \right) \frac{\partial w}{\partial y} \frac{\partial^2 w}{\partial y^2} + \left(A_{12} + A_{66} - \frac{B_{12} + B_{66}}{R} \right) \frac{\partial w}{\partial x} \frac{\partial^2 w}{\partial x \partial y}, \quad (31)$$

$$P_3(w) = 2(A_{12} + 2A_{66}) \frac{\partial w}{\partial x} \frac{\partial w}{\partial y} \frac{\partial^2 w}{\partial x \partial y} - \frac{w}{R} \left(A_{12} \frac{\partial^2 w}{\partial x^2} + A_{11} \frac{\partial^2 w}{\partial y^2} \right) + 2(B_{66} - B_{12}) \frac{\partial^2 w}{\partial x^2} \frac{\partial^2 w}{\partial y^2} + 2(B_{12} - B_{66}) \left(\frac{\partial^2 w}{\partial x \partial y} \right)^2 - \frac{A_{12}}{2R} \left(\frac{\partial w}{\partial x} \right)^2 - \frac{A_{11}}{2R} \left(\frac{\partial w}{\partial y} \right)^2 + \frac{3A_{11}}{2} \left[\frac{\partial^2 w}{\partial x^2} \left(\frac{\partial w}{\partial x} \right)^2 + \frac{\partial^2 w}{\partial y^2} \left(\frac{\partial w}{\partial y} \right)^2 \right] + \left(\frac{A_{12}}{2} + A_{66} \right) \left[\frac{\partial^2 w}{\partial y^2} \left(\frac{\partial w}{\partial x} \right)^2 + \frac{\partial^2 w}{\partial x^2} \left(\frac{\partial w}{\partial y} \right)^2 \right], \quad (32)$$

$$Q_3(u, w) = \left(\frac{\partial u}{\partial x} \frac{\partial^2 w}{\partial x^2} + \frac{\partial^2 u}{\partial x^2} \frac{\partial w}{\partial x} \right) + A_{12} \frac{\partial u}{\partial x} \frac{\partial^2 w}{\partial y^2} + A_{66} \frac{\partial w}{\partial x} \frac{\partial^2 u}{\partial y^2} + (A_{12} + A_{66}) \frac{\partial w}{\partial y} \frac{\partial^2 u}{\partial x \partial y} + 2A_{66} \frac{\partial u}{\partial y} \frac{\partial^2 w}{\partial x \partial y}, \quad (33)$$

$$R_3(v, w) = \left(A_{12} - \frac{B_{12}}{R} \right) \frac{\partial v}{\partial y} \frac{\partial^2 w}{\partial x^2} + 2 \left(A_{66} - \frac{B_{66}}{R} \right) \frac{\partial v}{\partial x} \frac{\partial^2 w}{\partial x^2} + \left(A_{11} - \frac{B_{11}}{R} \right) \left(\frac{\partial v}{\partial y} \frac{\partial^2 w}{\partial y^2} + \frac{\partial w}{\partial y} \frac{\partial^2 v}{\partial y^2} \right) + \left(A_{66} - \frac{B_{66}}{R} \right) \frac{\partial w}{\partial y} \frac{\partial^2 v}{\partial x^2} + \left(A_{12} + A_{66} - \frac{B_{12} + B_{66}}{R} \right) \frac{\partial w}{\partial x} \frac{\partial^2 v}{\partial x \partial y}. \quad (34)$$

3 Analytical solution

Many types of analytical and numerical methods are presented in the open literature to obtain a solution for the dynamic problems of continuous systems [80–86]. In this section, an analytical framework will be introduced to solve the governing equations of the problem. In this method, i.e., founded on the basis of Galerkin's technique, the displacement field components for a thin shell with both ends simply supported (S–S) will be considered as [77]:

$$\begin{aligned} u &= U(t) \cos \frac{m\pi x}{L} \sin \frac{ny}{R}, \\ v &= V(t) \sin \frac{m\pi x}{L} \cos \frac{ny}{R}, \\ w &= W(t) \sin \frac{m\pi x}{L} \sin \frac{ny}{R}, \end{aligned} \quad (35)$$

in which $U(t)$, $V(t)$, and $W(t)$ are the unknown Fourier coefficients regarding the oscillation amplitudes. Also, the longitudinal and circumferential half-mode numbers are

shown with m and n , respectively. If Eq. (35) is inserted into Eqs. (26)–(28), one can reach:

$$l_{11}U(t) + l_{12}V(t) + l_{13}W(t) + n_1W^2(t) = I_0 \frac{d^2U(t)}{dt^2}, \quad (36)$$

$$l_{21}U(t) + l_{22}V(t) + l_{23}W(t) + n_2W^2(t) = I_0 \frac{d^2V(t)}{dt^2}, \quad (37)$$

$$l_{31}U(t) + l_{32}V(t) + l_{33}W(t) + n_3W^2(t) + n_4W^3(t) + n_5U(t)W(t) + n_6V(t)W(t) + \frac{16q}{\pi^2 mn} = I_0 \frac{d^2W(t)}{dt^2} + 2\epsilon I_0 \frac{dW(t)}{dt}, \quad (38)$$

where

Table 1 Mechanical properties of the polymeric matrix and GFs [47]

E_{PM}^0	2.1 GPa
ν_{PM}^0	0.34
ρ_{PM}^0	1150 kg/m ³
E_F	71 GPa
G_F	30 GPa
ν_F	0.22
ρ_F	2450 kg/m ³

$$\begin{aligned}
 l_{11} &= -A_{11} \frac{\pi^2 m^2}{L^2} - A_{66} \frac{n^2}{R^2}, \\
 l_{12} = l_{21} &= \left(-A_{12} - A_{66} + \frac{B_{12} + B_{66}}{R} \right) \frac{\pi mn}{LR}, \\
 l_{13} = l_{31} &= -A_{12} \frac{\pi m}{LR} + B_{11} \frac{\pi^3 m^3}{L^3} + (B_{12} + 2B_{66}) \frac{\pi mn^2}{LR^2}, \\
 l_{22} &= \left(-A_{66} + \frac{2B_{66}}{R} - \frac{D_{66}}{R^2} \right) \frac{\pi^2 m^2}{L^2} + \left(-A_{11} + \frac{2B_{11}}{R} - \frac{D_{11}}{R^2} \right) \frac{\pi^2 m^2 n}{L^2 R}, \\
 l_{33} &= 2B_{12} \frac{\pi^2 m^2}{L^2 R} + 2B_{11} \frac{n^2}{R^3} - D_{11} \frac{\pi^4 m^4}{L^4} - D_{11} \frac{n^4}{R^4} - 2(D_{12} + 2D_{66}) \frac{\pi^2 m^2 n}{L^2 R^2} - \frac{A_{11}}{R^2} + \frac{ph\pi^2 m^2}{L^2}, \\
 n_1 &= -32A_{11} \frac{\pi m^2}{9L^3 n} + 16(-A_{11} - A_{66}) \frac{n}{9\pi LR^2}, \\
 n_2 &= \left(-A_{66} + A_{12} + \frac{B_{66} - B_{12}}{R} \right) \frac{16m}{9L^2 R} + \left(-A_{11} + \frac{B_{11}}{R} \right) \frac{32n^2}{9\pi^2 R^3 m}, \\
 n_3 &= 16A_{12} \frac{m}{3L^2 R n} + 16A_{11} \frac{n}{3\pi^2 R^3 m} + 32(B_{66} - B_{12}) \frac{mn}{3L^2 R^2}, \\
 n_4 &= -9A_{11} \frac{\pi^4 m^4}{32L^4} - (A_{12} + 2A_{66}) \frac{\pi^2 m^2 n^2}{16L^2 R^2} - 9A_{11} \frac{n^4}{32LR^2}, \\
 n_5 &= 32A_{11} \frac{\pi m^2}{9L^3 n} + 32(A_{12} - A_{66}) \frac{n}{9\pi LR^2}, \\
 n_6 &= \left(A_{12} - A_{66} + \frac{B_{66} - B_{12}}{R} \right) \frac{32m}{9L^2 R} + \left(A_{11} - \frac{B_{11}}{R} \right) \frac{32n^2}{9\pi^2 R^3 m}.
 \end{aligned} \tag{39}$$

In the nonlinear vibration problems with small oscillation amplitudes, it is logical to assume the in-plane inertia to be ignorable compared with the out-of-plane one [87]. Hence, Eqs. (36)–(38) can be re-written in the following form:

$$l_{11}U(t) + l_{12}V(t) + l_{13}W(t) + n_1W^2(t) = 0, \tag{40}$$

$$l_{21}U(t) + l_{22}V(t) + l_{23}W(t) + n_2W^2(t) = 0, \tag{41}$$

$$\begin{aligned}
 &l_{31}U(t) + l_{32}V(t) + l_{33}W(t) + n_3W^2(t) + n_4W^3(t) + n_5U(t)W(t) \\
 &+ n_6V(t)W(t) + \frac{16q}{\pi^2 mn} = I_0 \frac{d^2W(t)}{dt^2} + 2\epsilon I_0 \frac{dW(t)}{dt}.
 \end{aligned} \tag{42}$$

If $U(t)$ and $V(t)$ are extracted from simultaneous solution of Eqs. (40) and (41) in terms of $W(t)$ and $W^2(t)$ and thereafter substituted in Eq. (42), the following duffing equation will be achieved:

$$I_0 \frac{d^2W(t)}{dt^2} + 2\epsilon I_0 \frac{dW(t)}{dt} + a_1W(t) - a_2W^2(t) + a_3W^3(t) = \frac{16q}{\pi^2 mn}, \tag{43}$$

in which

$$\begin{aligned}
 a_1 &= -l_{33} - \frac{l_{31}(l_{12}l_{23} - l_{22}l_{13}) + l_{32}(l_{21}l_{13} - l_{11}l_{23})}{l_{11}l_{22} - l_{12}^2}, \\
 a_2 &= n_3 + \frac{l_{31}(l_{12}n_2 - l_{22}n_1) + l_{32}(l_{12}n_1 - l_{11}n_2) + n_5(l_{12}l_{23} - l_{22}l_{13}) + n_6(l_{12}l_{13} - l_{11}l_{23})}{l_{11}l_{22} - l_{12}^2}, \\
 a_3 &= -n_4 - \frac{n_5(l_{12}n_2 - l_{22}n_1) + n_6(l_{12}n_1 - l_{11}n_2)}{l_{11}l_{22} - l_{12}^2}.
 \end{aligned} \tag{44}$$

Table 2 Material properties of SWCNTs [51]

E_{CNT}	640(1 - 0.0005 ΔT) GPa
d_{CNT}	1.4×10^{-9} m
t_{CNT}	0.34×10^{-9} m
ρ_{CNT}	1350 Kg/m ³
l_{CNT}	25×10^{-6} m
ν_{CNT}	0.33

3.1 Linear frequency

It is possible to use Eqs. (36)–(38) to obtain linear natural frequency of the shell by ignoring nonlinear terms and the effect of the applied distributed load. The linear frequencies can be determined by solving the following eigenvalue system as [77]:

$$\begin{vmatrix} l_{11} + I_0\omega^2 & l_{12} & l_{13} \\ l_{21} & l_{22} + I_0\omega^2 & l_{23} \\ l_{31} & l_{32} & l_{33} + I_0\omega^2 \end{vmatrix} = 0. \tag{45}$$

Once the above identity is solved, the natural frequencies of the system will be attained. Among all of the triple frequencies, the smallest one will be the the fundamental frequency which is identical to $\omega_{mn} = \sqrt{a_1/I_0}$ that could be found earlier from Eq. (43).

3.2 Nonlinear forced vibration response

In this sub-section, it will be shown how to find the frequency–response relation of the present problem. In this work, a harmonic form will be considered for the distributed load applied on the edge of the shell. It is worth regarding that the harmonic excitation is presumed to be of the hard type. In other words, the load q is assumed to be $q = Q \sin \Omega t$ so that Ω denotes the excitation frequency. Once this type of dynamic stimulation is inserted into Eq. (43), the following expression can be achieved:

Table 3 Comparison of the nondimensional linear natural frequencies of metal foam shells

n	Ref. [88]	Ref. [89]	Present
1	1.2429	1.2466	1.2466
2	1.2387	1.2425	1.2425
3	1.2325	1.2366	1.2367
4	1.2256	1.2300	1.2302
5	1.2195	–	1.2246
6	1.2159	–	1.2216
7	1.2165	–	1.2228
8	1.2228	–	1.2298

Table 4 Comparison of dimensionless frequencies $\tilde{\omega} = \Omega(h/\pi)\sqrt{2(1 + \nu)\rho/E}$ of an isotropic cylindrical shell

(m,n)	Ref. [90]	Ref. [91]	Ref. [92]	Ref. [93]	Present
(1,1)	0.03692	0.03748	0.03739	0.03712	0.03760
(1,2)	0.03612	0.03671	0.03666	0.03648	0.03700
(1,3)	0.03566	0.03635	0.03634	0.03620	0.03680
(1,4)	0.03632	0.03720	0.03723	0.03700	0.03770

$$\frac{d^2W}{dt^2} + 2\varepsilon \frac{dW}{dt} + \omega_{mn}^2(W - HW^2 + KW^3) = F \sin \Omega t, \tag{46}$$

in which

$$F = \frac{16q}{\pi^2 mn}, \quad \omega_{mn} = \sqrt{a_1/I_0}, \quad H = \frac{a_2}{a_1}, \quad K = \frac{a_3}{a_1}. \tag{47}$$

To solve the problem, the method of harmonic balance will be utilized in this study. According to this method, the oscillation amplitude can be considered to be in a sinusoidal form as $W = A \sin \Omega t$. If this definition is substituted in Eq. (46), the identity will be enhanced as [77]:

$$\begin{aligned} \psi \equiv & A(\omega_{mn}^2 - \Omega^2) \sin \Omega t + 2\varepsilon A \Omega \cos \Omega t - \omega_{mn}^2 HA^2 \sin^2 \Omega t \\ & + K\omega_{mn}^2 A^3 \sin^3 \Omega t - F \sin \Omega t = 0. \end{aligned} \tag{48}$$

Once the product of the above identity in $\sin \Omega t$ is integrated with respect to time over a quarter of the oscillation period ($\int_0^{\pi/2\Omega} \psi \sin \Omega t dt = 0$), one can achieve:

$$\Omega^2 - \frac{4\varepsilon}{\pi} \Omega = \omega_{mn}^2 \left(1 - \frac{8}{3\pi} HA + \frac{3K}{4} A^2 \right) - \frac{F}{A}. \tag{49}$$

By defining $\alpha^2 = \Omega^2/\omega_{mn}^2$, Eq. (49) can be re-written as:

$$\alpha^2 - \frac{4\varepsilon}{\pi \omega_{mn}} \alpha = 1 - \frac{8}{3\pi} HA + \frac{3K}{4} A^2 - \frac{F}{A\omega_{mn}^2}. \tag{50}$$

The above relation is the frequency–response equation corresponding to the present system.

3.3 Nonlinear transient response

In this part of the solution, it will be tried to solve the problem in the time domain to reach the transient response of the MSH nanocomposite shell. To this purpose, Eq. (43) will be utilized. Once the fourth-order Runge–Kutta is applied to the mentioned relation and it is considered that the coefficients of the equation are functions of time due to the viscoelastic properties of the polymer, the time-varying expression for calculation of the dynamic deflection will be gathered.

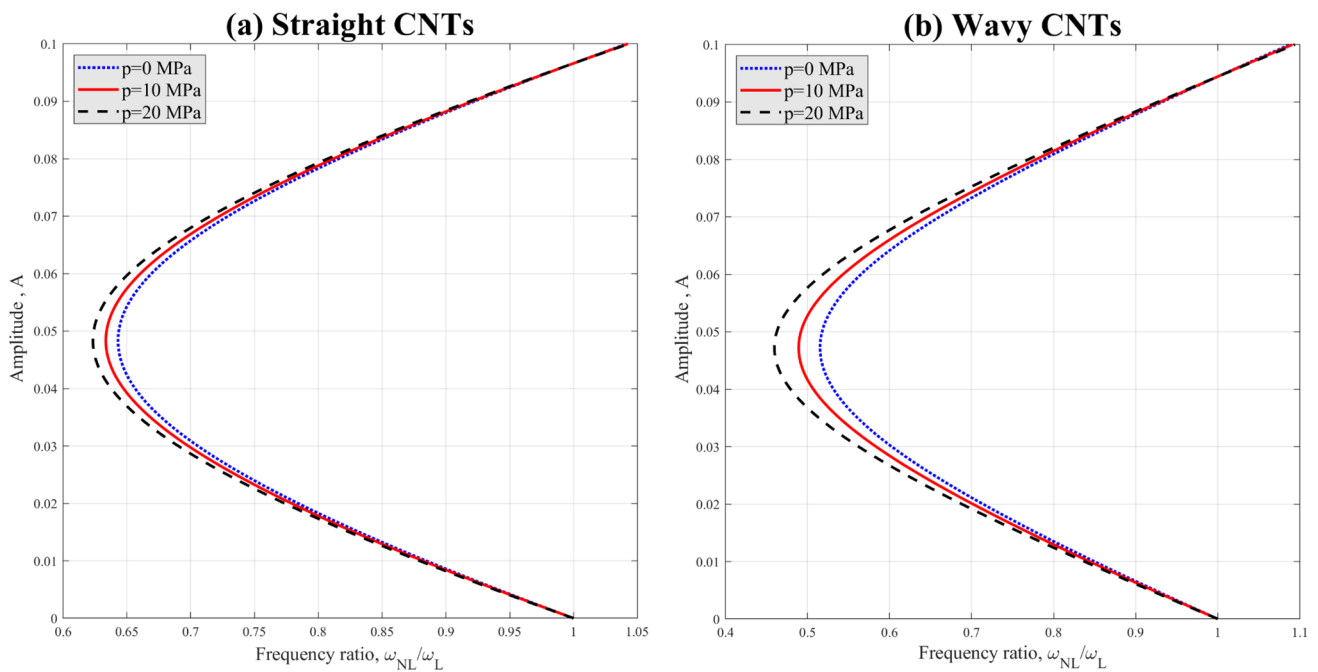


Fig. 2 Frequency–response curve of MSH nanocomposite shells subjected to various compressive loadings while (a) straight and (b) wavy nanofillers are utilized for the goal of reinforcement ($m_r=0.05$, $m_f=0.2$)

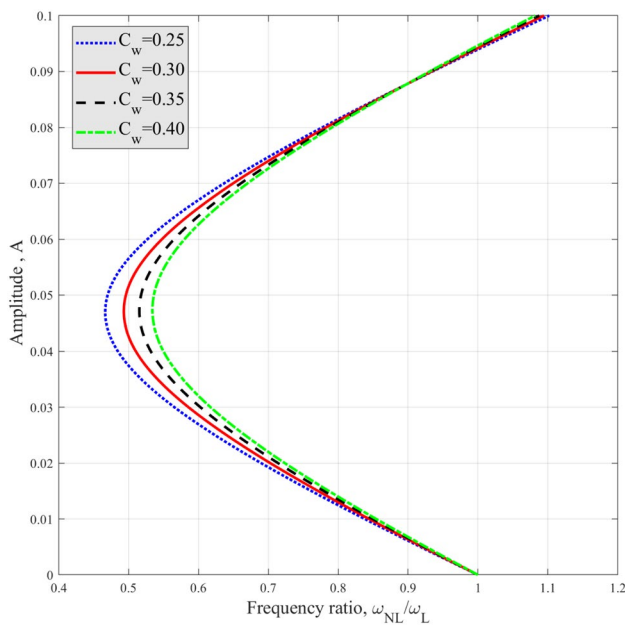


Fig. 3 Frequency–response curve of MSH nanocomposite shells for different values of waviness coefficient ($m_r=0.05$, $m_f=0.2$, $p=0$)

4 Results and discussion

Present part deals with numerical case studies revealing the most important findings of this study. In the following cases,

the radius-to-thickness ratio of the shell is assumed to be $R/h = 500$, to satisfy the assumption of thin-walled being of the structure. The entire thickness is fixed $h = 1$ mm, whereas the length of the shell is assumed to be two times its radius ($L/R = 2$). It is noteworthy that the stretching component and relaxation time are fixed on $\beta_v = 1$ and $\tau_v = 120$ s, respectively. Although the aforesaid inputs are considered in the following numerical cases, one can tailor the stretching component in the range of $0 < \beta_v < 1$ if it is supposed to monitor the viscoelastic behaviors of MSH nanocomposite shells in different damping rates. In addition, the material properties of the polymer and GF can be found in Table 1, whereas those of the CNTs are shown in Table 2.

4.1 Validation study

For the goal of being sure of the accuracy of the presented modeling, dynamic responses of cylindrical shells obtained from the present method are compared with those available in the literature. To this purpose, linear frequencies of metal foam shells reported in Refs. [88] and [89] are re-generated here. The results of this comparison can be found by referring to Table 3. Based on this comparison, the present method is able to approximate the vibrational characteristics of shell-type elements with a high precision. As another attempt toward validity check, the dimensionless frequencies of isotropic shells were calculated and are shown in Table 4.

Table 5 Effect of waviness coefficient C_w on natural frequencies (s^{-1}) of MSH nanocomposite shell ($p=0$, $t=0$)

C_w	$\omega_1 (m = 1, n = 3)$	$\omega_2 (m = 1, n = 1)$	$\omega_3 (m = 3, n = 3)$	$\omega_4 (m = 3, n = 1)$
0.20	847.38471	2656.9814	2658.3559	4817.1375
0.25	872.81522	2741.811	2743.1866	4905.4467
0.30	897.06752	2822.9047	2824.2833	4989.5068
0.35	920.28085	2900.6887	2902.0717	5069.919
0.40	942.57068	2975.5178	2976.9063	5147.163
0.45	964.03382	3047.6909	3049.0859	5221.6271
1.00	1162.6309	3719.5453	3721.0429	5920.5589

According to this table, our data are in an excellent agreement with those reported in Refs. [90–93].

4.2 Frequency–response curves

In this section of numerical results, frequency–response curves of the oscillating MSH nanocomposite structure will be depicted in the framework of Figs. 2–6. Based on Fig. 2, it can be simply perceived that the utilization of wavy CNTs leads to having a wider range for the frequency ratio in constant values of the system’s deflection. This trend means that the system behaves in a more flexible manner whenever curved nanofillers are employed as reinforcing gadgets. This figure also denotes that compressive pre-loading results in a reduction in the frequency ratio of the MSH nanocomposite shell, which can be referred to as a mechanical constraint.

To be familiar with the effect of waviness coefficient on the frequency–response curve of the nanocomposite shell, Fig. 3 is presented while there exists no compressive pre-loading. Based on this illustration, it can be confirmed that if big values are assigned to the waviness coefficient, a wider range of frequency ratio will be achieved. This trend is physically due to the fact that in such cases, the reinforcing nanofillers will be closer to their ideal straight shape. In other words, the amplitude of the existing wave in the CNTs’ chord will be smaller, while the waviness coefficient increases. So, it is recommended to choose waviness coefficients between 0.3 and 0.4, while it is aimed to have a safe approximation from the system’s behavior according to the experiments [45]. This finding can be observed in Tables 5 and 6, too. In these tables, the impact of the waviness coefficient on the linear natural frequency of the MSH nanocomposite shell is presented. According to Table 5, higher natural frequencies correspond to bigger waviness coefficients. Besides, Table 6 reveals that adding the time leads to a reduction in the frequency of the system because of the fact that in longer times, the stiffness of the polymeric matrix will be attenuated continuously.

In Figs. 4 and 5, the main concentration is on the investigation of the influences of GFs’ and CNTs’ mass fraction on the frequency–response curves of MSH nanocomposite shells, respectively. According to Fig. 4, it can be realized

that addition of the GFs’ mass fraction makes the frequency ratio wider, which might seem a little strange at the first glance. However, this effect is logical from physics viewpoint. In fact, a greater content of the macro-scale GFs corresponds with a reduction in the value of the nanofillers in the composition of the MSH nanomaterial. Hence, it is accurate to observe such a trend. In reverse, Fig. 5 indicates the positive role of the CNTs’ mass fraction on the frequency ratio of the vibrating nanocomposite structure. Based on this illustration, it can be figured out that the frequency ratio will be narrow if higher values are assigned to the mass fraction of the CNTs, thanks to the stiffness enhancement made in the nanomaterial.

As the final case study in this section, the combined effects of waviness phenomenon and excitation amplitude on the frequency–response curve of MSH nanocomposite shells are provided in Fig. 6. This diagram states that the deviation of the frequency–response curve from free oscillation case ($F = 0$) will be increased as the excitation amplitude is added. Also, it is clear that the tendency of the frequency–response curve of the system to the left side will be increased in the case of employing wavy CNTs for the purpose of manufacturing the hybrid nanomaterial. From our knowledge about nonlinear systems, it is obvious that this trend is a softening one that originated due to the destroying effect of the wavy shape of the nanofillers on the reinforcement mechanism in the nanocomposites. Hence, the resonance path of the fluctuating nanocomposite shell can be dramatically affected by the waviness phenomenon according to this diagram.

4.3 Transient response monitoring

Within this part of this manuscript, Figs. 7–10 will be studied whose major concern is to analyze the transient response of the vibrating system. In the first example, i.e., Fig. 7, the long-term behavior of the system is monitored. According to this figure, it is obvious that the mean value of the deflection amplitude will be decreased as time exceeds. The reason for this trend is the decreasing influence of time on the total stiffness of the polymeric matrix because of the viscoelastic nature of the polymers. Also, this diagram shows another

Table 6 Effect of time and circumferential wave number n on natural frequencies (s^{-1}) of MSH nanocomposite shell reinforced with both straight and wavy CNTs ($p=0$)

n	$t=0.00$		$t=0.02$		$t=0.04$		$t=0.06$		$t=0.08$		$t=0.10$	
	$C_w=0.35$	$C_w=1.00$	$C_w=0.35$	$C_w=1.00$	$C_w=0.35$	$C_w=1.00$	$C_w=0.35$	$C_w=1.00$	$C_w=0.35$	$C_w=1.00$	$C_w=0.35$	$C_w=1.00$
1	2900.6887	3719.5453	2900.5604	3719.4511	2900.4322	3719.3596	2900.304	3719.2627	2900.1758	3719.1686	2900.0476	3719.0744
2	1498.8794	1942.9627	1498.8099	1942.9106	1498.7405	1942.8585	1498.671	1942.8064	1498.6015	1942.7544	1498.5321	1942.7023
3	920.280085	1162.6309	920.24297	1162.6038	920.20509	1162.5766	920.16721	1162.5495	920.12934	1162.5224	920.09148	1162.4952
4	620.28325	762.68318	620.26132	762.668	620.23939	762.65283	620.21746	762.63766	620.19553	762.62249	620.17361	762.60732
5	448.25059	538.80618	448.23707	538.79697	448.22356	538.78775	448.21004	538.77854	448.19653	538.76933	448.18301	538.76012
6	349.41218	412.13309	349.4033	412.12702	349.39442	412.12095	349.38554	412.11489	349.37666	412.10882	349.36779	412.10276
7	301.78108	350.25976	301.77476	350.25538	301.76843	350.251	301.76211	350.24663	301.75579	350.24225	301.74947	350.23787
8	294.62239	337.7958	294.61731	337.79222	294.61222	337.78864	294.60713	337.78507	294.60205	337.78149	294.59696	337.77791
9	318.50973	362.52083	318.50497	362.51745	318.50021	362.51407	318.49545	362.51069	318.49069	362.50731	318.48593	362.50393
10	364.28411	413.10236	364.27909	413.09879	364.27408	413.09521	364.26907	413.0964	364.26405	413.08807	364.25904	413.0845

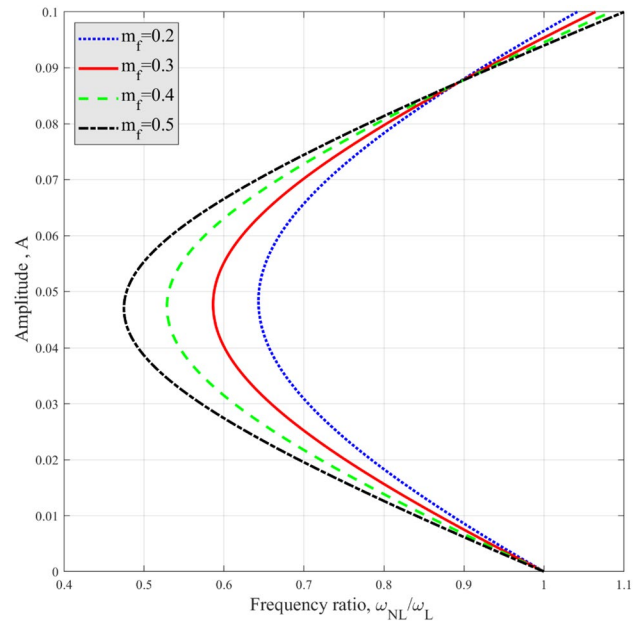


Fig. 4 Frequency–response curve of MSH nanocomposite shells reinforced with ideal (straight) CNTs for different values of GFs' mass fraction ($m_r=0.05$, $C_w=1$, $p=0$)

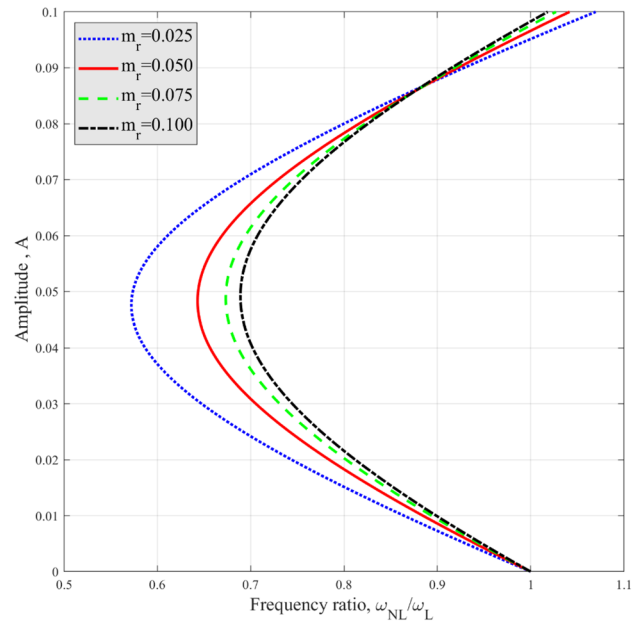


Fig. 5 Frequency–response curve of MSH nanocomposite shells reinforced with non-ideal (wavy) CNTs for different values of CNTs' mass fraction ($m_f=0.2$, $C_w=0.35$, $p=0$)

phenomenon. Indeed, it can be seen that over time, the variation of the deflection amplitude will be reduced because of the fact that the oscillator reaches its steady condition.

On the other hand, variation of the transient response of the system in a limited time interval can be observed

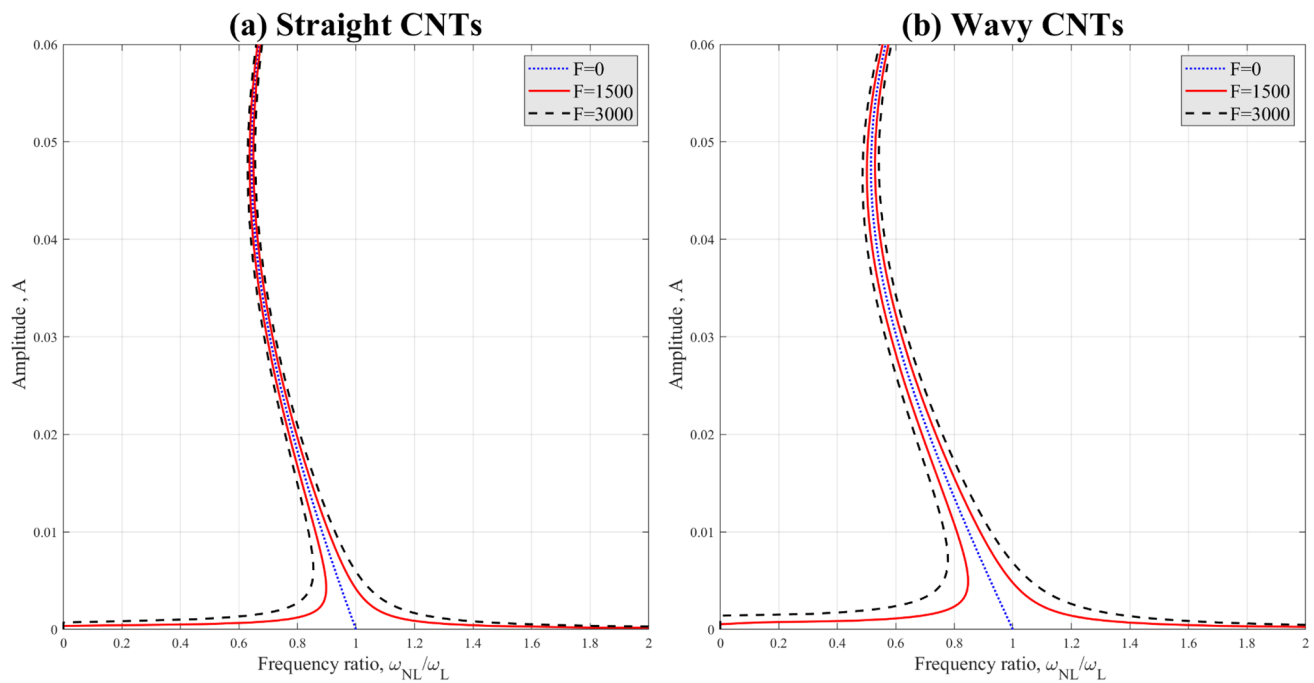


Fig. 6 Frequency–response curve of MSH nanocomposite shells for different values of loading amplitude F while (a) straight and (b) wavy CNTs are utilized for the goal of reinforcement ($m_r=0.05$, $m_j=0.2$)

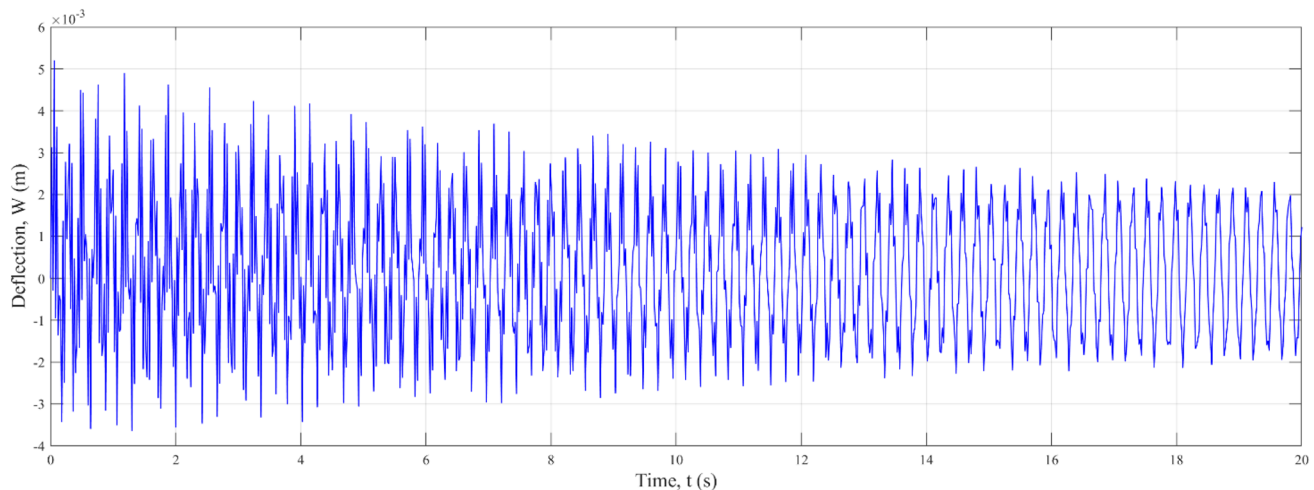


Fig. 7 Transient response of MSH nanocomposite subjected to a harmonic excitation once wavy CNTs are utilized for the goal of reinforcement ($C_w=0.35$, $m_r=0.05$, $m_j=0.2$, $F=1500$, $\Omega=600$)

in Fig. 8 whenever ideal and non-ideal CNTs are utilized in the composition of the hybrid nanomaterial. Based on this diagram, it is clear that the MSH nanocomposite shell experiences a beating-type oscillation. The small and big amplitudes of the system's beat are sensitive to the type of the reinforcing nanofillers. It is clear that if wavy CNTs are hired, the beating amplitude will be enlarged because of the negative impact of the waviness phenomenon on the stiffness of the three-phase nanomaterial. Also, the wavy shape of

the nanofillers induces a delay in the beating of the system, so that the number of beating cycles decreases in a constant time period if non-straight nanofillers are implemented in the manufacturing procedure.

Moreover, the effects of mass fraction of the macro- and nano-size reinforcing gadgets, namely GFs and CNTs, on the transient response of the MSH nanocomposite shells are shown in Figs. 9 and 10, respectively. According to these diagrams, it can be simply conceived that the addition of

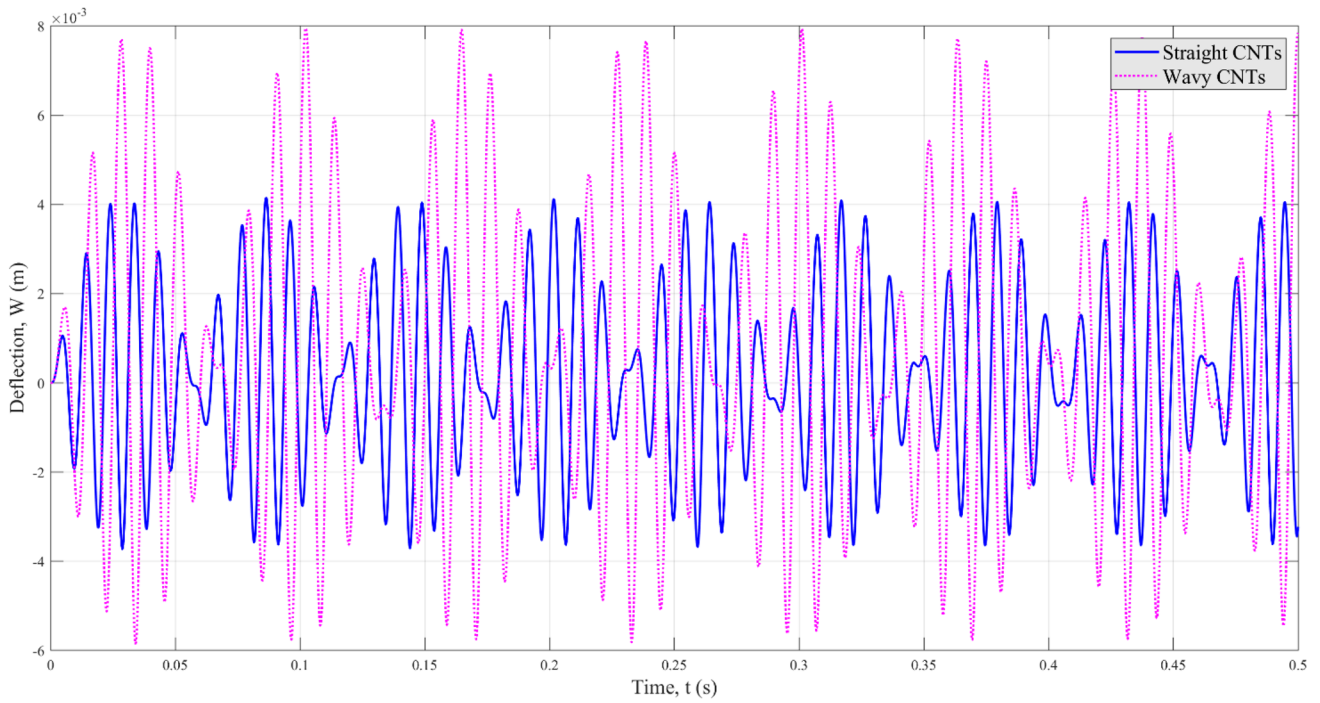


Fig. 8 Qualitative effect of the waviness phenomenon on the transient response of MSH nanocomposite shells ($m_r=0.1, m_f=0.2$)

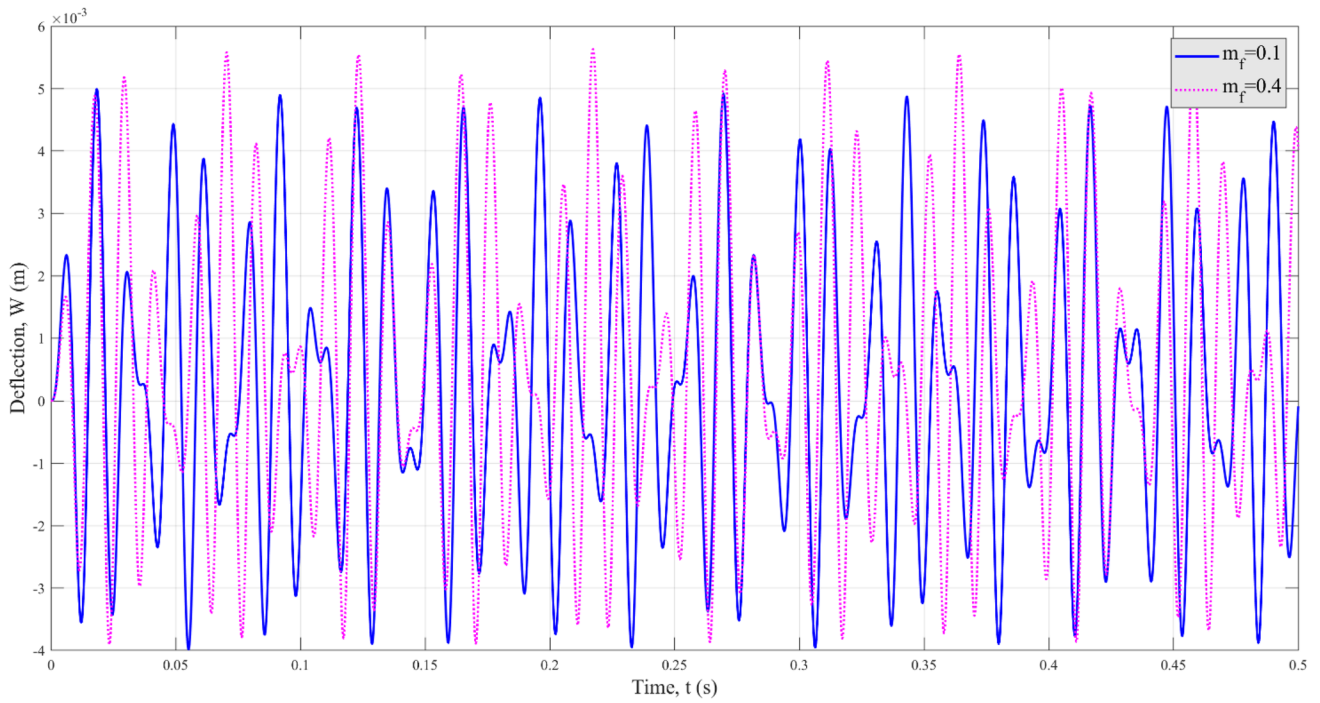


Fig. 9 Transient response of MSH nanocomposite shells reinforced via wavy CNTs for different values of GFs' mass fraction ($m_r=0.05, C_w=0.35$)

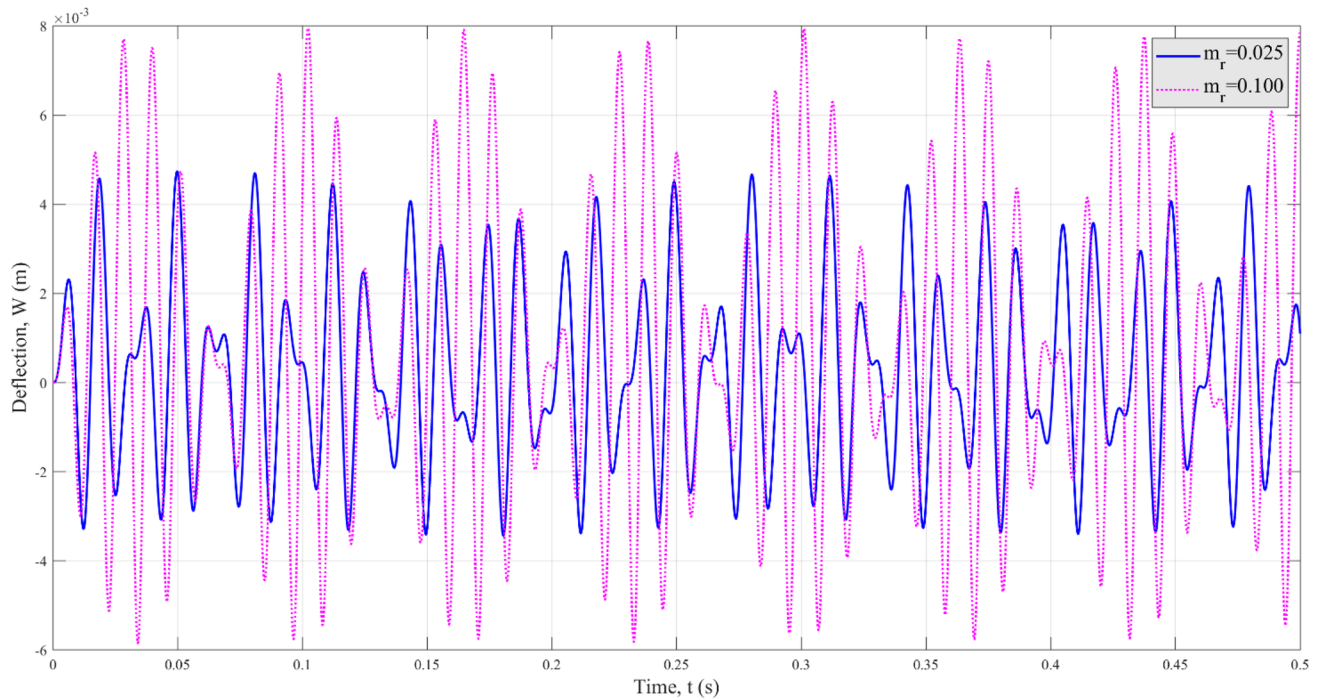


Fig. 10 Transient response of MSH nanocomposite shells reinforced via wavy CNTs for different values of CNTs' mass fraction ($m_r=0.2$, $C_w=0.35$)

the GFs' mass fraction intensifies the beating amplitude, whereas this parameter will be decreased if a greater content of the CNTs are hired in the fabrication procedure. The major reason of the first trend is that by adding the portion of the GFs in the hybrid nanomaterial, the content of the CNTs will be reduced because of the constant volume of the continua. Hence, it is natural to see such a softening behavior from physics point of view. Also, the observations of Fig. 10 can be physically justified by pointing out that addition of the content of the nanofillers stiffens the MSH nanocomposite.

5 Conclusion

This manuscript was majorly written to account for the coupled influences of the polymer's viscoelastic behavior and non-ideal shape of the CNTs on the nonlinear dynamic responses of thin-walled shells made from MSH nanocomposites. Herein, the most crucial highlights of this work will be reviewed in brief as below:

- It was shown that the dynamic amplitude of the system's beating diminished with increment of time. This trend physically appeared due to the viscoelastic features of the polymer.
- It was demonstrated that the nonlinear behavior of the shell is softer than the ideal theoretical estimations. This difference originates from the destructive impact of the waviness phenomenon on the mechanism of reinforcement in the hybrid nanomaterial.
- A limited rise in the mass fraction of the nanofillers is able to lessen the dynamic amplitude of deflection. The physical reason of this trend is enhancement of stiffness in MSH nanocomposites.
- Addition of the GFs' mass fraction resulted in a reduction in the equivalent stiffness of the MSH nanocomposite shell because it enforced the nanofillers' content to be decreased.
- It was illustrated that the existence of an axial compressive pre-load can lead to a wider range of nonlinear-to-linear frequency ratio in MSH nanocomposite shells through softening the structure.
- According to the utilized methodology, nonlinear dynamic characteristics of MSH nanocomposite shells are easy to reach without being involved in complex algebraic operations available in the method of multiple time scales.
- Finally, the presented micromechanical modeling makes it possible to estimate the mechanical properties of MSH nanocomposites, so that the guessed values are close to experimental data. Interestingly, this achievement is obtained with a very low-cost computational framework.

In addition to the above-mentioned positive aspects of this study, it is also crucial to point out the limitations of the present work. The effect of entanglement of CNTs in clusters on the Young's modulus is not covered in this work. Furthermore, the presented results are generated based on the assumption of the essence of ideal bonding between the nanofillers and matrix.

References

- Iijima S (1991) Helical microtubules of graphitic carbon. *Nature* 354(6348):56–58. <https://doi.org/10.1038/354056a0>
- Ruoff RS, Lorents DC (1995) Mechanical and thermal properties of carbon nanotubes. *Carbon* 33(7):925–930. [https://doi.org/10.1016/0008-6223\(95\)00021-5](https://doi.org/10.1016/0008-6223(95)00021-5)
- Xie S, Li W, Pan Z, Chang B, Sun L (2000) Mechanical and physical properties on carbon nanotube. *J Phys Chem Solids* 61(7):1153–1158. [https://doi.org/10.1016/S0022-3697\(99\)00376-5](https://doi.org/10.1016/S0022-3697(99)00376-5)
- Ajayan PM, Stephan O, Colliex C, Trauth D (1994) Aligned carbon nanotube arrays formed by cutting a polymer resin—nanotube composite. *Science* 265(5176):1212–1214. <https://doi.org/10.1126/science.265.5176.1212>
- Shen H-S, Zhang C-L (2010) Thermal buckling and postbuckling behavior of functionally graded carbon nanotube-reinforced composite plates. *Mater Des* 31(7):3403–3411. <https://doi.org/10.1016/j.matdes.2010.01.048>
- Shen H-S (2011) Postbuckling of nanotube-reinforced composite cylindrical shells in thermal environments. Part II: Pressure-loaded shells *Composite Structures* 93(10):2496–2503. <https://doi.org/10.1016/j.compstruct.2011.04.005>
- Wang Z-X, Shen H-S (2011) Nonlinear vibration of nanotube-reinforced composite plates in thermal environments. *Comput Mater Sci* 50(8):2319–2330. <https://doi.org/10.1016/j.commtsci.2011.03.005>
- Shen H-S, Xiang Y (2012) Nonlinear vibration of nanotube-reinforced composite cylindrical shells in thermal environments. *Comput Methods Appl Mech Eng* 213–216:196–205. <https://doi.org/10.1016/j.cma.2011.11.025>
- Wang Z-X, Shen H-S (2012) Nonlinear dynamic response of nanotube-reinforced composite plates resting on elastic foundations in thermal environments. *Nonlinear Dyn* 70(1):735–754. <https://doi.org/10.1007/s11071-012-0491-2>
- Zhu P, Lei ZX, Liew KM (2012) Static and free vibration analyses of carbon nanotube-reinforced composite plates using finite element method with first order shear deformation plate theory. *Compos Struct* 94(4):1450–1460. <https://doi.org/10.1016/j.compstruct.2011.11.010>
- Lei ZX, Liew KM, Yu JL (2013) Large deflection analysis of functionally graded carbon nanotube-reinforced composite plates by the element-free kp-Ritz method. *Comput Methods Appl Mech Eng* 256:189–199. <https://doi.org/10.1016/j.cma.2012.12.007>
- Rafiee M, Yang J, Kitipornchai S (2013) Thermal bifurcation buckling of piezoelectric carbon nanotube reinforced composite beams. *Comput Math Appl* 66(7):1147–1160. <https://doi.org/10.1016/j.camwa.2013.04.031>
- Rafiee M, Yang J, Kitipornchai S (2013) Large amplitude vibration of carbon nanotube reinforced functionally graded composite beams with piezoelectric layers. *Compos Struct* 96:716–725. <https://doi.org/10.1016/j.compstruct.2012.10.005>
- Ansari R, Faghhi Shojaei M, Mohammadi V, Gholami R, Sadeghi F (2014) Nonlinear forced vibration analysis of functionally graded carbon nanotube-reinforced composite Timoshenko beams. *Compos Struct* 113:316–327. <https://doi.org/10.1016/j.compstruct.2014.03.015>
- Heydarpour Y, Aghdam MM, Malekzadeh P (2014) Free vibration analysis of rotating functionally graded carbon nanotube-reinforced composite truncated conical shells. *Compos Struct* 117:187–200. <https://doi.org/10.1016/j.compstruct.2014.06.023>
- Rafiee M, He XQ, Liew KM (2014) Non-linear dynamic stability of piezoelectric functionally graded carbon nanotube-reinforced composite plates with initial geometric imperfection. *Int J Non-Linear Mech* 59:37–51. <https://doi.org/10.1016/j.ijnonlinmec.2013.10.011>
- Shen H-S, Xiang Y (2014) Postbuckling of axially compressed nanotube-reinforced composite cylindrical panels resting on elastic foundations in thermal environments. *Compos B Eng* 67:50–61. <https://doi.org/10.1016/j.compositesb.2014.06.020>
- Shen H-S, Xiang Y (2014) Nonlinear vibration of nanotube-reinforced composite cylindrical panels resting on elastic foundations in thermal environments. *Compos Struct* 111:291–300. <https://doi.org/10.1016/j.compstruct.2014.01.010>
- Zhang LW, Song ZG, Liew KM (2015) Nonlinear bending analysis of FG-CNT reinforced composite thick plates resting on Pasternak foundations using the element-free IMLS-Ritz method. *Compos Struct* 128:165–175. <https://doi.org/10.1016/j.compstruct.2015.03.011>
- Duc ND, Cong PH, Tuan ND, Tran P, Thanh NV (2017) Thermal and mechanical stability of functionally graded carbon nanotubes (FG CNT)-reinforced composite truncated conical shells surrounded by the elastic foundations. *Thin-Walled Structures* 115:300–310. <https://doi.org/10.1016/j.tws.2017.02.016>
- Duc ND, Lee J, Nguyen-Thoi T, Thang PT (2017) Static response and free vibration of functionally graded carbon nanotube-reinforced composite rectangular plates resting on Winkler-Pasternak elastic foundations. *Aerosp Sci Technol* 68:391–402. <https://doi.org/10.1016/j.ast.2017.05.032>
- Ebrahimi F, Farazmandnia N (2017) Thermo-mechanical vibration analysis of sandwich beams with functionally graded carbon nanotube-reinforced composite face sheets based on a higher-order shear deformation beam theory. *Mech Adv Mater Struct* 24(10):820–829. <https://doi.org/10.1080/15376494.2016.1196786>
- Memar Ardestani M, Zhang LW, Liew KM (2017) Isogeometric analysis of the effect of CNT orientation on the static and vibration behaviors of CNT-reinforced skew composite plates. *Comput Methods Appl Mech Eng* 317:341–379. <https://doi.org/10.1016/j.cma.2016.12.009>
- Civalek Ö, Baltacıoğlu AK (2018) Vibration of carbon nanotube reinforced composite (CNTRC) annular sector plates by discrete singular convolution method. *Compos Struct* 203:458–465. <https://doi.org/10.1016/j.compstruct.2018.07.037>
- Kiani Y, Mirzaei M (2018) Rectangular and skew shear buckling of FG-CNT reinforced composite skew plates using Ritz method. *Aerosp Sci Technol* 77:388–398. <https://doi.org/10.1016/j.ast.2018.03.022>
- Moradi-Dastjerdi R, Aghadavoudi F (2018) Static analysis of functionally graded nanocomposite sandwich plates reinforced by defected CNT. *Compos Struct* 200:839–848. <https://doi.org/10.1016/j.compstruct.2018.05.122>
- Thai CH, Ferreira AJM, Rabczuk T, Nguyen-Xuan H (2018) A naturally stabilized nodal integration meshfree formulation for carbon nanotube-reinforced composite plate analysis. *Eng Anal*

- Boundary Elem 92:136–155. <https://doi.org/10.1016/j.enganbound.2017.10.018>
28. Ansari R, Torabi J, Hassani R (2019) A comprehensive study on the free vibration of arbitrary shaped thick functionally graded CNT-reinforced composite plates. *Eng Struct* 181:653–669. <https://doi.org/10.1016/j.engstruct.2018.12.049>
 29. Chakraborty S, Dey T, Kumar R (2019) Stability and vibration analysis of CNT-Reinforced functionally graded laminated composite cylindrical shell panels using semi-analytical approach. *Compos B Eng* 168:1–14. <https://doi.org/10.1016/j.compositesb.2018.12.051>
 30. Jiao P, Chen Z, Li Y, Ma H, Wu J (2019) Dynamic buckling analyses of functionally graded carbon nanotubes reinforced composite (FG-CNTRC) cylindrical shell under axial power-law time-varying displacement load. *Compos Struct* 220:784–797. <https://doi.org/10.1016/j.compstruct.2019.04.048>
 31. Khosravi S, Arvin H, Kiani Y (2019) Interactive thermal and inertial buckling of rotating temperature-dependent FG-CNT reinforced composite beams. *Compos B Eng* 175:107178. <https://doi.org/10.1016/j.compositesb.2019.107178>
 32. Mehar K, Panda SK (2019) Theoretical deflection analysis of multi-walled carbon nanotube reinforced sandwich panel and experimental verification. *Compos B Eng* 167:317–328. <https://doi.org/10.1016/j.compositesb.2018.12.058>
 33. Bendenia N, Zidour M, Bousahla AA, Bourada F, Tounsi A, Benrahou KH, Bedia EAA, Mahmoud SR, Tounsi A (2020) Deflections, stresses and free vibration studies of FG-CNT reinforced sandwich plates resting on Pasternak elastic foundation. *Comput Concr* 26(3):213–226. <https://doi.org/10.12989/cac.2020.26.3.213>
 34. Civalek Ö, Avcar M (2020) Free vibration and buckling analyses of CNT reinforced laminated non-rectangular plates by discrete singular convolution method. *Eng Comput*. <https://doi.org/10.1007/s00366-020-01168-8>
 35. Moradi-Dastjerdi R, Behdinin K, Safaei B, Qin Z (2020) Buckling behavior of porous CNT-reinforced plates integrated between active piezoelectric layers. *Eng Struct* 222:111141. <https://doi.org/10.1016/j.engstruct.2020.111141>
 36. Ebrahimi F, Farazmandnia N, Kokaba MR, Mahesh V (2021) Vibration analysis of porous magneto-electro-elastically actuated carbon nanotube-reinforced composite sandwich plate based on a refined plate theory. *Eng Comput* 37(2):921–936. <https://doi.org/10.1007/s00366-019-00864-4>
 37. Zerrouki R, Karas A, Zidour M, Bousahla AA, Tounsi A, Bourada F, Tounsi A, Benrahou KH, Mahmoud SR (2021) Effect of nonlinear FG-CNT distribution on mechanical properties of functionally graded nano-composite beam. *Struct Eng Mech* 78(2):117–124. <https://doi.org/10.12989/sem.2021.78.2.117>
 38. Ghorbanpour Arani A, Kiani F, Afshari H (2021) Free and forced vibration analysis of laminated functionally graded CNT-reinforced composite cylindrical panels. *J Sandwich Struct Mater* 23(1):255–278. <https://doi.org/10.1177/1099636219830787>
 39. Zhang YY, Wang YX, Zhang X, Shen HM, She G-L (2021) On snap-buckling of FG-CNTR curved nanobeams considering surface effects. *Steel Compos Struct* 38(3):293–304. <https://doi.org/10.12989/scs.2021.38.3.293>
 40. Heidari F, Taheri K, Sheybani M, Janghorban M, Tounsi A (2021) On the mechanics of nanocomposites reinforced by wavy/defected/aggregated nanotubes. *Steel Compos Struct* 38(5):533–545. <https://doi.org/10.12989/scs.2021.38.5.533>
 41. Huang Y, Karami B, Shahsavari D, Tounsi A (2021) Static stability analysis of carbon nanotube reinforced polymeric composite doubly curved micro-shell panels. *Archives Civ Mech Eng* 21(4):139. <https://doi.org/10.1007/s43452-021-00291-7>
 42. Arshid E, Khorasani M, Soleimani-Javid Z, Amir S, Tounsi A (2021) Porosity-dependent vibration analysis of FG microplates embedded by polymeric nanocomposite patches considering hygrothermal effect via an innovative plate theory. *Eng Comput*. <https://doi.org/10.1007/s00366-021-01382-y>
 43. Zhang M, Li J (2009) Carbon nanotube in different shapes. *Mater Today* 12(6):12–18. [https://doi.org/10.1016/S1369-7021\(09\)70176-2](https://doi.org/10.1016/S1369-7021(09)70176-2)
 44. Ebrahimi F, Dabbagh A (2020) A brief review on the influences of nanotubes' entanglement and waviness on the mechanical behaviors of CNTR polymer nanocomposites. *Journal of Computational Applied Mechanics* 51 (1):247–252. Doi: <https://doi.org/10.22059/jcamech.2020.304476.517>
 45. Arasteh R, Omidi M, Rousta AHA, Kazerooni H (2011) A study on effect of waviness on mechanical properties of multi-walled carbon nanotube/epoxy composites using modified halpin-tsai theory. *J Macromol Sci Part B* 50(12):2464–2480. <https://doi.org/10.1080/00222348.2011.579868>
 46. Tornabene F, Fantuzzi N, Baccocchi M, Viola E (2016) Effect of agglomeration on the natural frequencies of functionally graded carbon nanotube-reinforced laminated composite doubly-curved shells. *Compos B Eng* 89:187–218. <https://doi.org/10.1016/j.compositesb.2015.11.016>
 47. Baccocchi M, Tarantino AM (2019) Time-dependent behavior of viscoelastic three-phase composite plates reinforced by Carbon nanotubes. *Compos Struct* 216:20–31. <https://doi.org/10.1016/j.compstruct.2019.02.083>
 48. Rafiee M, Liu XF, He XQ, Kitipornchai S (2014) Geometrically nonlinear free vibration of shear deformable piezoelectric carbon nanotube/fiber/polymer multiscale laminated composite plates. *J Sound Vib* 333(14):3236–3251. <https://doi.org/10.1016/j.jsv.2014.02.033>
 49. He XQ, Rafiee M, Mareishi S, Liew KM (2015) Large amplitude vibration of fractionally damped viscoelastic CNTs/fiber/polymer multiscale composite beams. *Compos Struct* 131:1111–1123. <https://doi.org/10.1016/j.compstruct.2015.06.038>
 50. Rafiee M, Nitzsche F, Labrosse M (2016) Rotating nanocomposite thin-walled beams undergoing large deformation. *Compos Struct* 150:191–199. <https://doi.org/10.1016/j.compstruct.2016.05.014>
 51. Ebrahimi F, Habibi S (2018) Nonlinear eccentric low-velocity impact response of a polymer-carbon nanotube-fiber multiscale nanocomposite plate resting on elastic foundations in hygrothermal environments. *Mech Adv Mater Struct* 25(5):425–438. <https://doi.org/10.1080/15376494.2017.1285453>
 52. Rafiee M, Nitzsche F, Labrosse MR (2018) Modeling and mechanical analysis of multiscale fiber-reinforced graphene composites: Nonlinear bending, thermal post-buckling and large amplitude vibration. *Int J Non-Linear Mech* 103:104–112. <https://doi.org/10.1016/j.ijnonlinmec.2018.05.004>
 53. Ebrahimi F, Dabbagh A (2019) Vibration analysis of graphene oxide powder-carbon fiber-reinforced multi-scale porous nanocomposite beams: a finite-element study. *Euro Phys J Plus* 134(5):225. <https://doi.org/10.1140/epjp/i2019-12594-1>
 54. Ebrahimi F, Dabbagh A (2021) An analytical solution for static stability of multi-scale hybrid nanocomposite plates. *Eng Comput* 37(1):545–559. <https://doi.org/10.1007/s00366-019-00840-y>
 55. Dabbagh A, Rastgoo A, Ebrahimi F (2020) Post-buckling analysis of imperfect multi-scale hybrid nanocomposite beams rested on a nonlinear stiff substrate. *Eng Comput*. <https://doi.org/10.1007/s00366-020-01064-1>
 56. Ebrahimi F, Dabbagh A, Rastgoo A (2020) Static stability analysis of multi-scale hybrid agglomerated nanocomposite shells.

- Mechanics Based Design of Structures and Machines:1–17. doi: <https://doi.org/10.1080/15397734.2020.1848585>
57. Ebrahimi F, Dabbagh A, Rastgoo A, Rabczuk T (2020) Agglomeration effects on static stability analysis of multi-scale hybrid nanocomposite plates. *Comput Materials Continua* 63(1):41–64. <https://doi.org/10.32604/cmc.2020.07947>
 58. Ebrahimi F, Dabbagh A (2020) Vibration analysis of multi-scale hybrid nanocomposite shells by considering nanofillers' aggregation. *Waves in Random and Complex Media*:1–19. <https://doi.org/10.1080/17455030.2020.1810363>
 59. Ebrahimi F, Dabbagh A, Rastgoo A (2021) Free vibration analysis of multi-scale hybrid nanocomposite plates with agglomerated nanoparticles. *Mech Based Des Struct Mach* 49(4):487–510. <https://doi.org/10.1080/15397734.2019.1692665>
 60. Ebrahimi F, Nopour R, Dabbagh A (2021) Effect of viscoelastic properties of polymer and wavy shape of the CNTs on the vibrational behaviors of CNT/glass fiber/polymer plates. *Eng Comput*. <https://doi.org/10.1007/s00366-021-01387-7>
 61. Ferry JD (1980) *Viscoelastic Properties of Polymers*. 3rd edn. John Wiley & Sons,
 62. Drozdov AD, Kalamkarov AL (1996) A constitutive model for nonlinear viscoelastic behavior of polymers. *Polym Eng Sci* 36(14):1907–1919. <https://doi.org/10.1002/pen.10587>
 63. Brinson HF, Brinson LC (2008) *Polymer Engineering Science and Viscoelasticity*. 1st edn. Springer, Boston, MA, USA. doi: <https://doi.org/10.1007/978-0-387-73861-1>
 64. Cox HL (1952) The elasticity and strength of paper and other fibrous materials. *Br J Appl Phys* 3(3):72–79. <https://doi.org/10.1088/0508-3443/3/3/302>
 65. Aboutalebi R, Eshaghi M, Taghvaeipour A (2021) Nonlinear vibration analysis of circular/annular/sector sandwich panels incorporating magnetorheological fluid operating in the post-yield region. *J Intell Mater Syst Struct* 32(7):781–796. <https://doi.org/10.1177/1045389X20975471>
 66. Mobasheri Zafarabadi MM, Aghdam MM (2021) Semi-analytical solutions for buckling and free vibration of composite anisogrid lattice cylindrical panels. *Compos Struct* 275:114422. <https://doi.org/10.1016/j.compstruct.2021.114422>
 67. Ebrahimi F, Nopour R, Dabbagh A (2021) Smart laminates with an auxetic ply rested on visco-Pasternak medium: active control of the system's oscillation. *Eng Comput*. <https://doi.org/10.1007/s00366-021-01533-1>
 68. Aboutalebi R, Eshaghi M, Taghvaeipour A, Bakhtiari-Nejad F (2021) Post-Yield characteristics of electrorheological fluids in nonlinear vibration analysis of smart sandwich panels. *Mechanics Based Design of Structures and Machines*:1–20. doi:<https://doi.org/10.1080/15397734.2021.1886946>
 69. Al-Furjan MSH, Habibi M, Ni J, Dw J, Tounsi A (2020) Frequency simulation of viscoelastic multi-phase reinforced fully symmetric systems. *Eng Comput*. <https://doi.org/10.1007/s00366-020-01200-x>
 70. She G-L (2021) Guided wave propagation of porous functionally graded plates: The effect of thermal loadings. *J Therm Stresses* 44(10):1289–1305. <https://doi.org/10.1080/01495739.2021.1974323>
 71. She G-L, Liu H-B, Karami B (2021) Resonance analysis of composite curved microbeams reinforced with graphene nanoplatelets. *Thin-Walled Struct* 160:107407. <https://doi.org/10.1016/j.tws.2020.107407>
 72. Ding H-X, She G-L (2021) A higher-order beam model for the snap-buckling analysis of FG pipes conveying fluid. *Struct Eng Mech* 80(1):63–72. <https://doi.org/10.12989/sem.2021.80.1.063>
 73. Lu L, She G-L, Guo X (2021) Size-dependent postbuckling analysis of graphene reinforced composite microtubes with geometrical imperfection. *Int J Mech Sci* 199:106428. <https://doi.org/10.1016/j.ijmecsci.2021.106428>
 74. Xiao H, Yan K, She G (2021) Study on the characteristics of wave propagation in functionally graded porous square plates. *Geomech Eng* 26(6):607–615. <https://doi.org/10.12989/gae.2021.26.6.607>
 75. Ebrahimi F, Dabbagh A (2021) Magnetic field effects on thermally affected propagation of acoustical waves in rotary double-nanobeam systems. *Waves Random Complex Media* 31(1):25–45. <https://doi.org/10.1080/17455030.2018.1558308>
 76. Ebrahimi F, Dabbagh A, Rabczuk T (2021) On wave dispersion characteristics of magnetostrictive sandwich nanoplates in thermal environments. *Eur J Mech A Solids* 85:104130. <https://doi.org/10.1016/j.euromechsol.2020.104130>
 77. Bich DH, Xuan Nguyen N (2012) Nonlinear vibration of functionally graded circular cylindrical shells based on improved Donnell equations. *J Sound Vib* 331(25):5488–5501. <https://doi.org/10.1016/j.jsv.2012.07.024>
 78. Ebrahimi F, Dabbagh A (2020) *Mechanics of Nanocomposites: Homogenization and Analysis*. 1st edn. CRC Press, Boca Raton, FL, USA. doi: <https://doi.org/10.1201/9780429316791>
 79. Ebrahimi F, Dabbagh A (2019) *Wave Propagation Analysis of Smart Nanostructures*. 1st edn. CRC Press, Boca Raton, FL, USA. doi: <https://doi.org/10.1201/9780429279225>
 80. Ebrahimi F, Hosseini SHS, Bayrami SS (2019) Nonlinear forced vibration of pre-stressed graphene sheets subjected to a mechanical shock: An analytical study. *Thin-Walled Structures* 141:293–307. <https://doi.org/10.1016/j.tws.2019.04.038>
 81. Karimiasl M, Ebrahimi F (2019) Large amplitude vibration of viscoelastically damped multiscale composite doubly curved sandwich shell with flexible core and MR layers. *Thin-Walled Structures* 144:106128. <https://doi.org/10.1016/j.tws.2019.04.020>
 82. Karimiasl M, Ebrahimi F, Mahesh V (2019) Nonlinear forced vibration of smart multiscale sandwich composite doubly curved porous shell. *Thin-Walled Struct* 143:106152. <https://doi.org/10.1016/j.tws.2019.04.044>
 83. Safarpour M, Ghabussi A, Ebrahimi F, Habibi M, Safarpour H (2020) Frequency characteristics of FG-GPLRC viscoelastic thick annular plate with the aid of GDQM. *Thin-Walled Structures* 150:106683. <https://doi.org/10.1016/j.tws.2020.106683>
 84. Yarali E, Farajzadeh MA, Noroozi R, Dabbagh A, Khoshgoftar MJ, Mirzaali MJ (2020) Magnetorheological elastomer composites: Modeling and dynamic finite element analysis. *Compos Struct* 254:112881. <https://doi.org/10.1016/j.compstruct.2020.112881>
 85. Soleimani H, Goudarzi T, Aghdam MM (2021) Advanced structural modeling of a fold in Origami/Kirigami inspired structures. *Thin-Walled Structures* 161:107406. <https://doi.org/10.1016/j.tws.2020.107406>
 86. Kabir H, Aghdam MM (2021) A generalized 2D Bézier-based solution for stress analysis of notched epoxy resin plates reinforced with graphene nanoplatelets. *Thin-Walled Structures* 169:108484. <https://doi.org/10.1016/j.tws.2021.108484>
 87. Fallah A, Aghdam MM (2012) Thermo-mechanical buckling and nonlinear free vibration analysis of functionally graded beams on nonlinear elastic foundation. *Compos B Eng* 43(3):1523–1530. <https://doi.org/10.1016/j.compositesb.2011.08.041>
 88. Wang Y, Wu D (2017) Free vibration of functionally graded porous cylindrical shell using a sinusoidal shear deformation theory. *Aerosp Sci Technol* 66:83–91. <https://doi.org/10.1016/j.ast.2017.03.003>

89. Wang YQ, Ye C, Zu JW (2019) Nonlinear vibration of metal foam cylindrical shells reinforced with graphene platelets. *Aerosp Sci Technol* 85:359–370. <https://doi.org/10.1016/j.ast.2018.12.022>
90. Bhimaraddi A (1984) A higher order theory for free vibration analysis of circular cylindrical shells. *Int J Solids Struct* 20(7):623–630. [https://doi.org/10.1016/0020-7683\(84\)90019-2](https://doi.org/10.1016/0020-7683(84)90019-2)
91. Lam KY, Loy CT (1995) Effects of boundary conditions on frequencies of a multi-layered cylindrical shell. *J Sound Vib* 188(3):363–384. <https://doi.org/10.1006/jsvi.1995.0599>
92. Xuebin L (2008) Study on free vibration analysis of circular cylindrical shells using wave propagation. *J Sound Vib* 311(3):667–682. <https://doi.org/10.1016/j.jsv.2007.09.023>
93. Shen H-S (2012) Nonlinear vibration of shear deformable FGM cylindrical shells surrounded by an elastic medium. *Compos Struct* 94(3):1144–1154. <https://doi.org/10.1016/j.compstruct.2011.11.012>

Publisher's Note Springer Nature remains neutral with regard to jurisdictional claims in published maps and institutional affiliations.